Astronomy & Astrophysics manuscript no. C60˙folding
March 17, 2015

Top-down formation of fullerenes in the interstellar medium

O. Berné[1,2], J. Montillaud[3,4] and C. Joblin[1,2]

[1] Université de Toulouse; UPS-OMP; IRAP; Toulouse, France
[2] CNRS; IRAP; 9 Av. colonel Roche, BP 44346, F-31028 Toulouse cedex 4, France
[3] Department of Physics, PO Box 64, University of Helsinki, 00014, Helsinki, Finland
[4] Institut Utinam, CNRS UMR 6213, OSU THETA, Université de Franche-Comté, 41bis avenue de l'Observatoire, 25000 Besançon, France

Received August ??, 2012; accepted ??, 2012

ABSTRACT

Fullerenes have recently been detected in various circumstellar and interstellar environments, raising the question of their formation pathway. It has been proposed that they can form at the low densities found in the interstellar medium by the photo-chemical processing of large polycyclic aromatic hydrocarbons (PAHs). Following our previous work on the evolution of PAHs in the NGC 7023 reflection nebula, we evaluate, using photochemical modelling, the possibility that the PAH $C_{66}H_{20}$ (i.e. circumovalene) can lead to the formation of C_{60} upon irradiation by ultraviolet photons. The chemical pathway involves full dehydrogenation of $C_{66}H_{20}$, folding into a floppy closed cage and shrinking of the cage by loss of C_2 units until it reaches the symmetric C_{60} molecule. At 10" from the illuminating star and with realistic molecular parameters, the model predicts that 100% of $C_{66}H_{20}$ is converted into C_{60} in $\sim 10^5$ years, a timescale comparable to the age of the nebula. Shrinking appears to be the kinetically limiting step of the whole process. Hence, PAHs larger than $C_{66}H_{20}$ are unlikely to contribute significantly to the formation of C_{60}, while PAHs containing between 60 and 66 C atoms should contribute to the formation of C_{60} with shorter timescales, and PAHs containing fewer than 60 C atoms will be destroyed. Assuming a classical size distribution for the PAH precursors, our model predicts that absolute abundances of C_{60} are up to several 10^{-4} of the elemental carbon, that is, less than a percent of the typical interstellar PAH abundance, which is consistent with observational studies. According to our model, once formed, C_{60} can survive much longer ($> 10^7$ years for radiation fields below $G_0 = 10^4$) than other fullerenes because of the remarkable stability of the C_{60} molecule at high internal energies. Hence, a natural consequence is that C_{60} is more abundant than other fullerenes in highly irradiated environments.

Key words. astrochemistry - ISM: molecules - molecular processes - Methods: numerical

1. Introduction

The mid-infrared (mid-IR) spectrum of galactic and extragalactic objects exhibits emission in bands (strongest at 3.3, 6.2, 7.7, 8.6, and 11.2 μm) attributed to carbonaceous macromolecules, more specifically, to polycyclic aromatic hydrocarbons (PAHs, Tielens 2008). In addition to PAH bands, IR emission bands at 7.0, 8.5, 17.4, and 19.0 μm have been reported (Cami et al. 2010; Sellgren et al. 2010) and found to match the IR active bands of neutral buckminsterfullerene quite closely (C_{60}, Kroto et al. 1985). Buckminsterfullerne is a cage-like carbon molecule. Additional bands at 6.4, 7.1, 8.2, and 10.5 μm were observed in the NGC 7023 reflection nebula and attributed to the C_{60}^+ cation (Berné et al. 2013). Carbonaceous macromolecules, especially PAHs, are believed to play a fundamental role in the physics and chemistry of the interstellar medium (ISM), and their infrared signatures are commonly used as a tracer of physical conditions (especially the UV radiation field). PAHs are believed to lock up between 5 and 20% of the elemental carbon (Joblin & Tielens 2011), while C_{60} and $C_{60}^+$are found in small abundances in the ISM (at most 5.6×10^{-4} of the elemental carbon for the neutral form according to Castellanos et al. 2014, and at most 10^{-4} of the elemental carbon for the cation according to Berné et al. 2013). Nevertheless, C_{60} and C_{60}^+ are the only species belonging to the family of carbonaceous macromolecules that have been specifically identified in the ISM, and therefore these molecules have attracted considerable interest because they open a new possibility to probe carbon chemistry and physical conditions in the ISM.

One question related to fullerenes, and in particular C_{60} , concerns their formation pathway. Recently, "top-down" schemes where larger carbon clusters shrink to reach C_{60} have been proposed (Chuvilin et al. 2010; Zhang et al. 2013; Pietrucci & Andreoni 2014), and can be opposed to the traditional "bottom-up" approach where C_{60} is built up from small compounds (Kroto & McKay 1988; Heath 1992; Hunter et al. 1994; Dunk et al. 2013). Using infrared observations of the NGC 7023 nebula, Berné & Tielens (2012) found evidence of an increase of the abundance of C_{60} with increasing UV field, while the abundance of PAHs decreases. This was interpreted by these authors as evidence for the formation of C_{60} from large PAHs ($N_C > 60$) under UV irradiation, a top-down mechanism similar to the one observed by Chuvilin et al. (2010). García-Hernández et al. (2010, 2011) and Micelotta et al. (2012) proposed a similar mechanism where the starting materials are more complex, such as hydrogenated amorphous carbon instead of PAHs. Top-down scenarios are particularly appealing, given that the densities prevailing in the ISM are many orders of magnitude too low to allow for a bottom-up formation (i.e. starting from small compounds) over reasonable timescales[1]. In this paper, we use a detailed photochemical model coupled to a description of the physical con-

[1] While writing the present paper, it was proposed by Patra et al. (2014) that nucleation of C atoms leading to the formation of cages can operate in the ISM. However, the densities and relative abundances of C

ditions in the NGC 7023 nebula. We demonstrate that the formation of C_{60} by UV processing of large PAH molecules is a plausible mechanism to account for astronomical observations.

2. Model for the formation of C_{60} from PAHs

2.1. Description of the proposed scenario

The proposed scenario of formation is inspired by the one described in Berné & Tielens (2012) and is represented schematically in Fig. 1. PAHs are assumed to be formed in the envelopes of evolved stars (Frenklach & Feigelson 1989; Cherchneff et al. 1992; Merino et al. 2014) and then to be injected in the ISM. Under UV irradiation, large PAHs, ($N_C > 60$) are first fully dehydrogenated into small graphene flakes, dehydrogenation being by far the dominant dissociation channel (see Montillaud et al. 2013, and references therein). Additional UV irradiation enables these flakes to fold into closed cages. Once the cages are closed, they can loose C_2 units if they continue to absorb energy (Irle et al. 2006). Because of the low densities prevailing in the considered regions ($n_H < 10^4 \mathrm{cm}^{-3}$), the reverse reaction, that is, addition of C_2 , is too slow to balance photodissociation. Once a system has reached C_{60} , it will remain in this form for a very long time because it is remarkably stable.

2.2. Specific case of the transformation of $C_{66}H_{20}$ into C_{60}

We consider the evolution of circumovalene, $C_{66}H_{20}$ (first molecule in Fig. 1), for the physical conditions of NGC 7023 (see Sect. 3). We restrict ourselves to a single molecule as a starting point for simplicity and because modelling a complete population would introduce many free parameters that would be irrelevant in this proof-of-concept study. $C_{66}H_{20}$ is selected as a test case because it gathers the typical properties expected for an interstellar PAH ($N_C \gtrsim 50$, compactness), it can be considered as a potential precursor of C_{60} , and its spectroscopic properties are available in the Cagliari theoretical spectral database of PAHs[2] (Malloci et al. 2007, hereafter Cagliari database). The photophysical modelling relies on several key processes: 1) UV absorption, which brings the molecules to high temperatures, 2) radiative cooling, 3) unimolecular dissociation, 4) isomerization and more specifically, folding of the graphene flakes, and 5) reactions with electrons, H atoms, or C^+. In the following sections, we present the adopted methods to describe these processes, which were then implemented in the photochemical model developed by Montillaud et al. (2013).

2.2.1. UV absorption

UV absorption is the first step in the photophysical evolution of the considered species. The efficiency of this process in a given radiation field depends on the UV absorption cross-section. The UV absorption cross-section of $C_{66}H_{20}$ used here is taken from the Cagliari database. The same value is used for dehydrogenated PAHs $C_{66}H_n$ and for planar C_{66}, considering that the UV absorption cross-section in a PAH is, in first approximation, proportional to the number of carbon atoms. For C_{60} , we adopted the UV absorption cross-section from Berkowitz (1999). The same absorption cross-section was used for the other cages, but with a scaling proportional to the number of C atoms (Joblin et al. 1992). The impact of the chosen UV absorption cross-sections on the results is discussed in Sect. 4.3.

2.2.2. Ionization

In the frame of our interstellar model, two ionization processes need to be considered: direct photoionization, and thermionic emission. Direct ionization occurs after the absorption of a single UV photon with an energy above the ionization threshold. In the case of thermionic emission, the successive absorption of several UV photons brings the molecule to high temperatures and can lead to delayed electron emission.

For the hydrogenated and dehydrogenated PAHs, the direct photoionization process was included, following Montillaud et al. (2013). For the cages, including C_{60} , we did not include direct photoionization. This assumption relies on the fact that observations indicate that this species is mostly in the neutral form in NGC 7023, C_{60}^+being localized only very close to the star (Berné et al. 2013). It cannot be excluded that this is due to an efficient recombination of C_{60} with electrons from the ambient medium, and hence ionization could still be efficient as a sink of energy for relaxation. Since the ionization potential of C_{60} is 7.5 eV, only photons with energies $7.5 < h\nu < 13.6$ eV can contribute to ionization. Given the spectral profile of the radiation field in NGC 7023 (see Montillaud et al. 2013) and the fact that in this range the ionization yield is lower than the total photo-absorption (Berkowitz 1999), only a small fraction of the energy from absorbed UV photons will be lost in photoelectrons, and most of it will be converted into vibrational energy that can eventually be used for dissociation. The other cages have similar ionization potentials (Seifert et al. 1996) and were therefore assumed to behave like C_{60} . Hence, we have neglected direct photoionizaiton for the cages in the photo-chemical model.

Thermionic emission becomes efficient only at internal energies higher than $\sim$ 30 eV (Hansen et al. 2003). It could therefore be an efficient relaxation process, competing with photodissociation (Sect. 2.2.4) and cooling by fluorescence from thermally excited electronic states (Sect. 2.2.3). As can be seen in Fig. 2, the thermionic emission rate becomes higher than fluorescence from thermally excited electronic states only for internal energies above $\sim$ 45 eV. This is well above the internal energies of dissociation (see Sect. 4.1), and therefore relaxation through thermionic emission can be neglected since it will always be dominated by fluorescence from thermally excited electronic states.

2.2.3. Radiative cooling

Radiative cooling can occur through emission of photons in the infrared, but when the molecules reach high enough temperatures, it has been shown that fluorescence from thermally excited electronic states becomes the dominant cooling mechanism (see Léger et al. 1988, who called this mechanism Poincaré fluorescence). This process has been observed for internal energies of $\sim$ 7 eV for the anthracene cation, $C_{14}H_{10}^+$, (Martin et al. 2013) and internal energies of $\sim$ 13 eV for the C_{60} anion (Andersen et al. 2001).

The infrared cooling rates were calculated using the microcanonical formalism of Joblin et al. (2002). This requires the full knowledge of the vibrational properties of the considered species. For $C_{66}H_{20}$, we used the spectroscopic properties from the Cagliari database as in Montillaud et al. (2013). For C_{60} , they were taken from Schettino et al. (2001). For dehydrogenated

and H adopted in this latter work are far different from those considered here and from what is observed in the interstellar medium.

[2] astrochemistry.ca.astro.it/database/

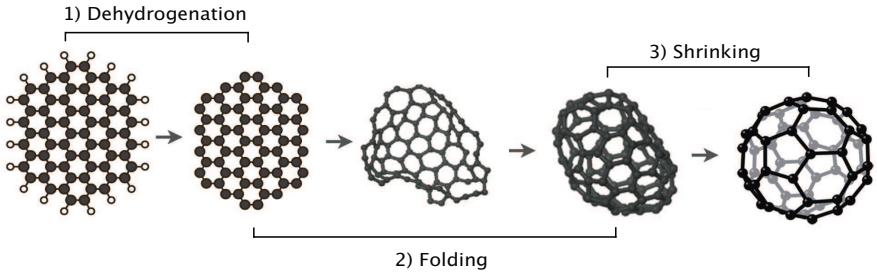

Fig. 1. Schematic representation of the evolutionary scenario for the formation of fullerenes from PAHs under UV irradiation.

Table 1. Frequencies and oscillator strengths adopted in the approximation to calculate the cooling by fluorescence from thermally excited electronic states (see text for details).

λ (Å)	ν_i (Hz)	f_i
	$C_{66}H_{20}$	
5470	5.48×10^{14}	0.72
4980	6.02×10^{14}	0.24
	C_{60}	
4540	6.60×10^{14}	0.214
3485	8.60×10^{14}	1.17
2725	1.10×10^{15}	2.02
2240	1.34×10^{15}	1.30

PAHs $C_{66}H_n$ and cages, we used the DFT vibrational frequencies of $C_{66}H_{20}$ from the Cagliari database, after removing the C-H vibrational modes and three modes per missing C atom. The cooling rates calculated with this approach for C_{60} are reported in Fig. 2.

Cooling by fluorescence from thermally excited electronic states was calculated using the formalism described in Chupka & Klots (1997). The cooling rate is given by

$$k(T) = (2c/a_0) \sum f_i (h\nu_i/mc^2)^2 \, exp(-h\nu_i/k_B T), \quad (1)$$

where a_0 is the Bohr radius, f_i and ν_i are the oscillator strengths and frequencies of the electronic transitions, and T is the temperature of the molecule. For $C_{66}H_{20}$ and for the dehydrogenated PAHs we used the ν_i and f_i values for $C_{66}H_{20}$ from the Cagliari database (Table 1). For the cages, we used the energies and oscillator strengths of C_{60} taken from Chupka & Klots 1997, reproduced in Table 1. Note that these oscillator strengths are a convenient approximation to calculate the radiative cooling, but are not true oscillator strengths. Nevertheless, Chupka & Klots (1997) have shown that this approximation agrees very well with rate calculations that include detailed molecular property information. Using the microcanonical formalism described above to calculate the IR cooling rates, we derived the relation between internal energy E and temperature T for the different species. Using Eq. 1, this allowed us to derive the radiative cooling rates as a function of E. For C_{60} these rates are shown in Fig. 2) and agree well with the earlier work models of Tomita et al. (2003).

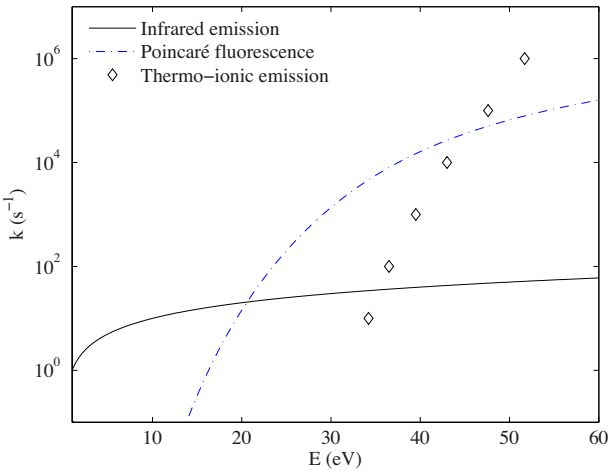

Fig. 2. Cooling rates for C_{60} as a function of the internal energy of the molecule. The infrared emission and cooling by fluorescence from thermally excited electronic states are calculated (labelled Poincaré in the figure) following the formalism described in this paper. The thermionic emission rates are taken from Hansen et al. (2003).

2.2.4. Photodissociation: dehydrogenation and shrinking by loss of C_2

Photodissociation was treated using the statistical approach and was based on the inverse Laplace transform of the Arrhenius equation (see details in Montillaud et al. 2013 and references therein). The parameters involved in this calculation are the activation energy E_0, the pre-exponential factor A, and the vibrational densities of states that are computed using the vibrational frequencies. For PAH dehydrogenation (first step in Fig. 1), we used the parameters given in Montillaud et al. (2013). For the shrinking of cages by loss of C_2 molecules (step 3 in Fig. 1), experimental and theoretical results are scarce, except for C_{60} and C_{60}^+, for which published molecular data have a large scatter, as noted by Matt et al. (2001). These authors reanalysed published experiments of C_{60}^+ dissociation and showed that when using similar and consistent sets of molecular data, most experiments lead to similar results, with a pre-exponential factor of $5{\times}10^{19}$s^{-1} and a dissociation energy of 10.0 ± 0.2 eV. The activation energy should be equal to the dissociation energy if there is no barrier for the reverse reaction, that is, C_2 addition. Experimental

(Laskin et al. 1997) and theoretical (Yi & Bernholc 1993) studies indeed indicate the absence of such a barrier. More recent studies are generally in line with these results (Diaz-Tendero et al. 2003; Gluch et al. 2004, among others). We considered each shrinking step from C_{66} to C_{58} individually (Eqs. 2 to 6 in Table 2). Dissociation energies were determined theoretically (Zhang et al. 1992), and the values differ significantly from experimental data (Gluch et al. 2004). The theoretical values were computed directly for neutral cages in a consistent manner for all species. In contrast, the experimental values were derived from measurements on fullerene cations. We used the theoretical values in our standard model (Table 2). This choice has the advantage of providing consistent energies for all cages in this study, but with a slightly higher value for C_{60} (11.1 eV) than in the results of Matt et al. (2001) (10.0 eV). To reconcile our choice of binding energies with the results of Matt et al. (2001), we adopted a pre-exponential factor of $2 \times 10^{20} s^{-1}$, which leads to a dissociation rate comparable to that of Matt et al. (1999) (their Fig. 8). We used the same factor for the C_2 loss of all cages. The impact of all these assumptions is discussed in Sect. 4.3.

2.2.5. Folding

For the folding of the carbon flakes (step 2 in Fig. 1), there are, to our knowledge, no experimental data to constrain the activation energy and pre-exponential factors. Recently, Lebedeva et al. (2012) conducted molecular dynamics simulations of the folding of the C_{96} and C_{384} graphene nanoflakes. For these two systems, they ran simulations at several temperatures and found that the rates follow an Arrhenius law from which they were able to derive the effective activation energies and pre-exponential factors. They showed that these parameters do not vary significantly with size[3], hence we adopted their values reported for C_{96} to describe the folding (see Table 2).

2.2.6. Reaction with electrons, H atoms, or C^+

The other processes of interest include the recombination with electrons and the reaction with H atoms. During the dehydrogenation step, all these processes were included, following Montillaud et al. (2013). We did not include the addition of C_2 because the abundance of this species is expected to be very low in the cavity of NGC 7023. The C^+ cation is abundant, however, and could react efficiently with cages. There are to our knowledge no studies of the kinetics of this reaction. We estimated the maximum contribution of this process in the case of C_{60} using the Langevin rate. A polarizability of ~ 80 Å^3 for C_{60} (Zope et al. 2008) leads to $k_{\rm Langevin} \sim 6 \times 10^{-9}$ cm^{3}s^{-1}, and assuming a high abundance of C^+ of $3 \times 10^{-4}\, n_{\rm H}$, this yields an effective C^+ addition rate of $\sim 2 \times 10^{-12}\, n_{\rm H}$ s^{-1} (that is $< 4 \times 10^{-8}$ s^{-1} for $n_H < 2 \times 10^4$cm^{-3}). This rate must be compared to the rate of the reverse process, that is, to photodissociation of C_{61}^+. We modelled this latter process with the same formalism as described in Sect. 3, using a dissociation energy of 4 eV (Slanina & Lee 1994) and a pre-exponential factor of 1.6×10^{15} s^{-1} (Klots 1991). We find photodissociation rates from $\sim 7 \times 10^{-8}$ s^{-1} to $\sim 2 \times 10^{-5}$ s^{-1} for the various astrophysical conditions considered in Sect. 4.2. Therefore, the photodissociation of C_{61} is estimated to be generally much faster than C^+ addition in the regions of interest, and we did not include this latter process in our study.

[3] This assertion concerns the range of 100-400 C atoms and may not extend to lower C numbers, but as discussed in Sect. 4.3, the activation energy would need to be different from the energy adopted here by a large factor to alter our results.

Table 2. Activation energy and pre-exponential factors for the key reactions considered in the model

		Act. energy E_a (eV)	Pre-exp. factor A (s^{-1})
(1)	$C_{66}^{planar} \rightarrow C_{66}^{cage}$	4.0	1×10^{15}
(2)	$C_{66}^{cage} \rightarrow C_{64}^{cage} + C_2$	8.1^a / 9.4^b	2×10^{20}
(3)	$C_{64}^{cage} \rightarrow C_{62}^{cage} + C_2$	9.4^a / 9.0^b	2×10^{20}
(4)	$C_{62}^{cage} \rightarrow C_{60}^{cage} + C_2$	6.0^a / 8.1^b	2×10^{20}
(5)	$C_{60}^{cage} \rightarrow C_{58}^{cage} + C_2$	11.1^a / 11.2^b	2×10^{20}
(6)	$C_{58}^{cage} \rightarrow C_{56}^{cage} + C_2$	8.7^a / 9.7^b	2×10^{20}

Notes. a. Using activation energies of Zhang et al. (1992); b. Using activation energies of Gluch et al. (2004).

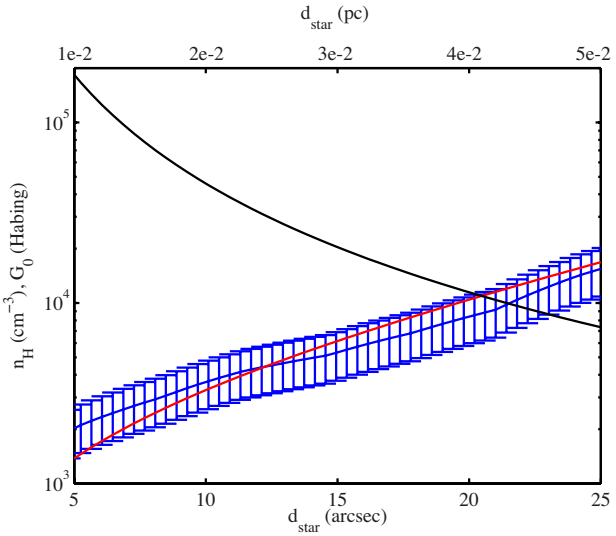

Fig. 3. Physical conditions in NGC 7023. Density profile derived from observations of the far-infrared dust emission in the cavity of NGC 7023 (blue with error-bars) and exponential fit to this profile used in the photochemical model (red line). The black line shows the adopted profile for the intensity of the radiation field G_0.

3. Astrophysical environment: NGC 7023

Since NGC 7023 is the template interstellar source for the study of fullerene formation (Sellgren et al. 2010; Berné & Tielens 2012; Montillaud et al. 2013), we modelled the photochemical evolution of $C_{66}H_{20}$ for conditions found in this nebula. The formation of C_{60} is thought to occur inside the cavity between the star HD 200775 and the PDR situated 40" at the north-west of the star. Here, we studied five positions at 5, 10, 15, 20, and 25" from the star, situated on a cross-cut (see Fig. 1 in Montillaud et al. 2013) that extends from the star to the PDR. On the same cross-cut, we derived the spectral energy distribution (SED) of dust emission using archival data from the *Herschel* space telescope (see Abergel et al. 2010). Using these SEDs, we derived the column density on the line of sight using a value for dust opacity at 250 μm of 1.14×10^{-25}cm^2 per H atom (see details on the method in Planck Collaboration XXV 2011). This yields a

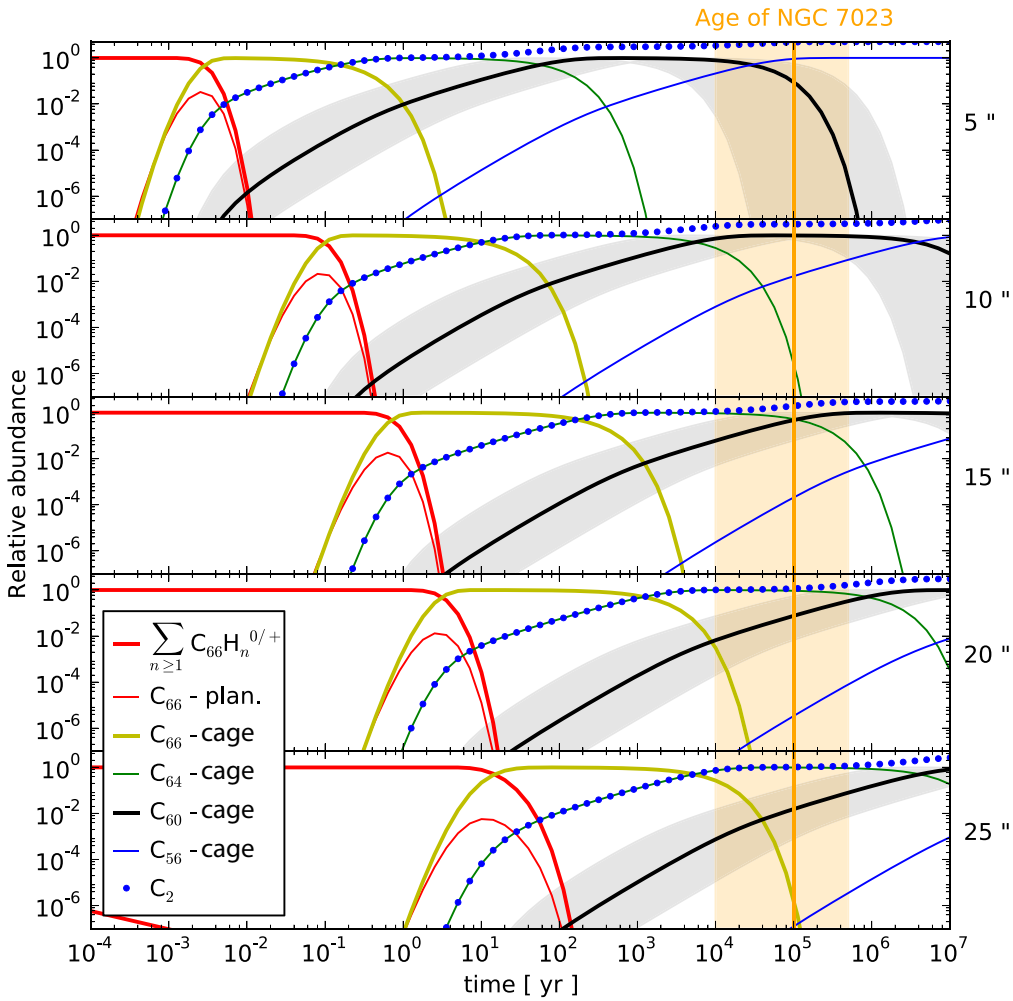

Fig. 5. Model results for the time-evolution of the abundance of PAHs ($\sum_{n=1}^{20} C_{66}H_n$), cages ($C_{66}^{planar}$, C_{66}^{cage}, C_{64}^{cage},C_{62}^{cage}, C_{60}^{cage}, C_{58}^{cage}), and C_2. These are normalized to the abundance of $C_{66}H_{20}$ at $t = 0$. The model calculations are made for distances of 5, 10, 15, 20, and 25" from the star HD 200775 in NGC 7023. Note that the dissociation of C_2 is not treated in our model, hence the C_2 abundances reported are only provided as an indication of how much C_2 is formed from the dissociation of cages. Similarly, the dissociation of the C_{56}^{cage} is not included in the model and therefore its abundance is provided as an indication of how much C_{60} is being destroyed. The grey shadowed regions indicate the uncertainty range implied by uncertainties of a factor of 10 on the rates of C_2 loss (see Sect. 4.3 for details). The approximate age of NGC 7023 is given, with orange shadowed regions representing the uncertainty on this value (see Sect. 3 for details).

column density profile, which we divided by the thickness of the region derived by Pilleri et al. (2012) based on the modelling of the PAH emission profile, that is, 0.13 pc. The resulting density profile is shown in Fig. 3. To obtain an analytical description of this profile, we fitted it with an exponential law (see Fig. 3). The intensities of the radiation field at 5, 10, 15, 20, and 25" from the star were derived as in Montillaud et al. (2013) and the corresponding profile of G_0 (UV field intensity in terms of the Habing field, which corresponds to 1.6×10^{-3} erg cm^{-2} s^{-1} when integrated between 91.2 and 240 nm, Habing 1968) as a function of distance to the star is presented in Fig. 3. To derive the temperature of the gas at these positions, PDR modelling is required. For the conditions described above, the gas temperature derived by the Meudon PDR model typically ranges between a few 100 and 1000 K. Here we adopted a characteristic temperature of 300 K for the photochemical model, but the exact value is not important (see Sect. 4.3). Finally, the age of the nebula is a key parameter for comparing the results of the model with observations. This begins with the time at which the cloud started to receive UV photons. This number cannot be derived directly, and hence other indicators have to be used. One is the age of the illuminating star HD 200775. It is difficult to give a precise "age" for such a young and massive star, but it most likely ranges between 10^4 and 5×10^5 years (Alecian et al. 2008, 2013 and Alecian 2014 priv. comm.). Berné & Tielens (2012) adopted a value for the age of the nebula ranging from a few 10^4 to 1×10^5 years. The analysis of the dynamical properties of the warm neutral gas traced by the C^+ line with Herschel indicate an age of ~ 0.5 Myr (Berné et al. 2012). However, more recent calculations focusing on the photo-evaporation flow in the NGC 7023 northern PDR indicate ages as young as 1.6×10^4 years (Berné et al. in prep). We used 10^5 years as the reference age, but we considered a range between 10^4 and 5×10^5 as an age uncertainty range.

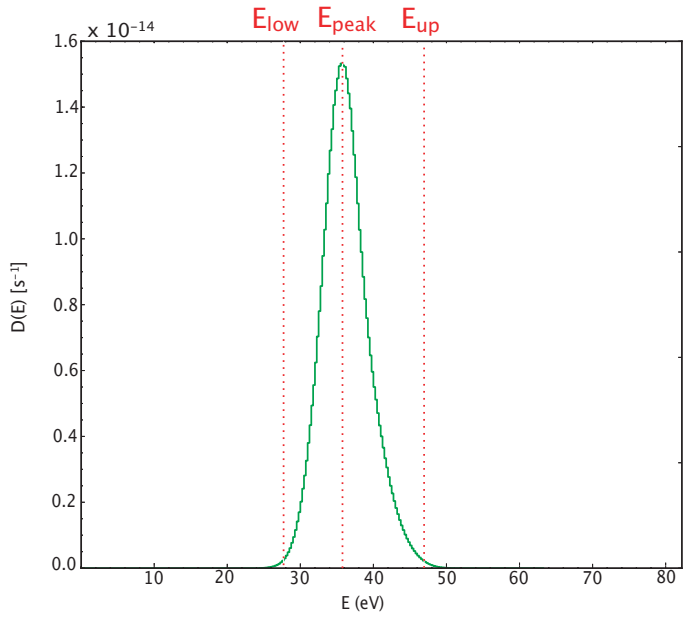

Fig. 4. Probability density function of dissociation of the C_{60} molecule as a function of internal energy, at a distance of 5" from the star ($G_0 \sim 2 \times 10^5$). Energies E_{peak} at the highest dissociation rate ($D(E) = k_{diss}(E) \times n(E)$), E_{low} and E_{up} (where $D(E_{up}) = D(E_{low}) = D(E_{peak})/100$ and $E_{up} > E_{low}$) are depicted. The values of E_{peak}, E_{low} and E_{up} for all cages are given in Table 3.

4. Results

4.1. Internal energies

To understand the processes at play in the photochemistry, it is useful to evaluate the probability density functions (PDFs) of the internal energies of the species that photodissociate with the model. Figure 4 shows such a PDF for C_{60} at a distance of 5" from the star. In Table 3, we report the main characteristics of these PDFs for all the cages considered in the model: the peak energy E_{peak} , that is, the energy of highest dissociation rate $D(E)$ expressed in s^{-1}, and the lower and upper bounds E_{low} and E_{up} defined by $D(E_{up}) = D(E_{low}) = D(E_{peak})/100$ with $E_{up} > E_{low}$ (see Fig. 4 for a graphical definition of these parameters). These values were calculated using the activation energies of Zhang et al. (1992) and those of Gluch et al. (2004) (Table 2). The results presented in Table 3 indicate that the internal energies required to dissociate the molecules are high, > 15 eV. Photons in the NGC 7023 nebula have a maximum energy set by the Lyman limit, 13.6 eV. Hence, the molecules that dissociate must have absorbed multiple photons, and therefore the photochemistry of these species is completely governed by these multiple-photon absorptions. In the specific case of C_{60} , the energy needed is at least 27 eV, which means that it requires the absorption of at least three photons to dissociate.

4.2. Abundances

The results of the model are given in Fig. 5, which presents the time-evolution of the abundance of PAHs ($\sum_{n=1}^{20} C_{66}H_n$), cages ($C_{66}^{planar}$, C_{66}^{cage} , C_{64}^{cage} ,C_{62}^{cage} , C_{60}^{cage} , C_{58}^{cage}), and C_2, at distances of 5, 10, 15, 20, and 25" from the star HD 200775 in NGC 7023. For these five positions, full dehydrogenation occurs very quickly (a few 10s of years at 25" and a few days at 5" from the star). This implies that $C_{66}H_{20}$ is quickly destroyed in NGC 7023, but larger PAHs could survive over longer timescales. Once the planar C_{66} is formed, it immediately folds and forms a cage. This implies that graphene flakes are only transient species and therefore unlikely to be detected in the ISM. The C_{64} cage, instead, can survive for a relatively long period (few 10s of years at 5" from the star and up to several 10^5 years at 25" from the star). This means that the shrinking step, where cages loose C_2 units, limits the efficiency of the C_{60} formation process in this model. Since each of the C_2 loss processes is time consuming, it appears unlikely that PAHs with sizes $N_C \gtrsim 66$ C atoms will contribute significantly to the formation of C_{60} . At distances shorter than 10" from the star, the cages can shrink to C_{60} , and after 10^5 years, all the $C_{66}H_{20}$ has been converted to C_{60} . Once the molecules have reached C_{60}, it takes a very long time to destroy them: C_{60} survives for 10's of Myr at distance larger than 10" from the star (radiation fields below G_0 of a few 10^4). Only at the closest position to the star (5", $G_0 \sim 2 \times 10^5$) is C_{60} destroyed efficiently, and hence it is predicted that its abundance will decrease after a few 10^4 years.

Table 3. Properties of the probability density functions of dissociation of cages (see an example of such a function in Fig. 4) : E_{peak}, E_{low} and E_{up}. All values in eV and derived for a distance of 5" from the star ($G_0 \sim 2 \times 10^5$).

	a.			b.		
Species*	E_{low}	E_{peak}	E_{up}	E_{low}	E_{peak}	E_{up}
C_{66}	22	32	39	26	35	43
C_{64}	24	35	43	24	34	41
C_{62}	15	20	28	22	30	36
C_{60}	27	36	47	27	36	47
C_{58}	22	30	37	24	33	41

Notes. *Only cages are presented in this table. a. Using activation energies of Zhang et al. (1992); b. Using activation energies of Gluch et al. (2004).

4.3. Sensitivity of model results

Is the model very sensitive to the adopted parameters, and if so, which are the critical parameters ?

First, we have checked that the dehydrogenation timescale is always much shorter than the cage formation plus shrinking timescale for the physical conditions of the considered positions. Therefore, it is equivalent to start our calculations with the planar C_{66} rather than with $C_{66}H_{20}$. All the following tests have been conducted with the above assumption, except for the gas temperature test. We first tested the choice in the vibrational frequencies for the system. We found that the exact values of the frequencies have a negligible effect on the results as long as the number of vibrational degrees of freedom and the orders of magnitude of the frequencies are correct. We varied the gas temperature in the model from 100 to 300 and 1000 K and found that this has a negligible impact on the C_{60} formation timescale. The UV-visible absorption cross -section of the cages, which is not well known, has a slightly stronger effect on the results. For instance, if we were to use for the cages the cross-section per C atom of $C_{66}H_{20}$ (Malloci et al. 2007) instead of the cross-section of C_{60} (Berkowitz 1999), we would obtain a variation by a factor of three in the timescale of formation of C_{60}. When we multiplied the pre-exponential factors of C_2 loss by 0.1 or 10

simultaneously for all cages, we observed an inversely proportional variation of the C_{60} formation timescale. This effect on the abundance of C_{60} is illustrated by the shadowed region in Fig. 5. When we varied these coefficients individually, we found that the results are mainly affected by the value for $C_{66} \rightarrow C_{64} + C_2$ and marginally for $C_{64} \rightarrow C_{62} + C_2$, while changes for the two other shrinking reactions did not affect the results. We compared our standard results (i.e. using the activation energies from Zhang et al. 1992) with the results obtained using the experimental dissociation energies of Gluch et al. (2004). The C_{60} formation timescales were slightly increased, mainly becaues of the higher stability of C_{66}^{cage} in the experimental data set. Overall, the effect does not affect the comparison with observations and discussion that follows. We therefore only consider the results of the model using the activation energies from Zhang et al. 1992 below. The main source of uncertainty appears to arise from the pre-exponetial factors chosen for the shrinking steps. We therefore consider their effect in the comparison with observations.

5. Comparison with observations

In this section we compare the results of our model with the observation of C_{60} formation in NGC 7023. To be completely accurate, this comparison would require that the model contains a whole size distribution of PAHs in agreement with observations. This requirement is beyond the scope of this paper, but the agreement between the observations and the model can be tested bearing this limitation in mind.

The comparison is primarily based on comparing the highest abundance of C_{60} observed in NGC 7023, at a distance of 11" from the star, with the value obtained in the model for a distance of 10". Taking into account the uncertainty on the age of NGC 7023 and the uncertainty on the pre-exponential factors, the model-predicted abundances of C_{60} ranges between a lowest value of 1.3×10^{-2} and 0.98, relative to $C_{66}H_{20}$ (Fig. 5). To convert this into an absolute abundance of C_{60} , one needs to know the abundance of $C_{66}H_{20}$ relative to the total PAH population and the total abundance PAHs in NGC 7023. The latter was estimated by Berné & Tielens (2012) to be $f_C^{PAH} = 7 \times 10^{-2}$ expressed as the fraction of carbon locked in PAHs. The highest abundance of $C_{66}H_{20}$ relative to the total PAH population, α, was estimated following Pilleri et al. (2009), using the PAH size distribution of Desert et al. (1990), which yields a value $\alpha = 5.3 \times 10^{-3}$. Thus, the fraction of carbon locked in $C_{66}H_{20}$ is $5.3 \times 10^{-3} \times 7 \times 10^{-2} = 3.7 \times 10^{-4}$. With this value, the fraction of carbon locked in C_{60} predicted by the model at a distance of 10" from the star ranges between $f_C^{C_{60}} = 4.8 \times 10^{-6}$ and $f_C^{C_{60}} = 3.6 \times 10^{-4}$ (where the lower and upper limit of the range include the uncertainty on the pre-exponential factor and the age of the nebula). This range of values agrees with the range derived by Berné & Tielens (2012) of $f_C^{C_{60}} = 1.7 \times 10^{-4}$. So far, we have considered $C_{66}H_{20}$ as the only precursor of C_{60} . As mentioned in Sect. 4.2, it is reasonable to expect that only PAHs bearing between 60 and 66 C-atoms will be able to form C_{60} and hence can increase the final abundance of C_{60}. This means that it is realistic to calculate α incorporating all the species bearing between 60 and ~66 C atoms, which yields $\alpha = 3.8 \times 10^{-2}$. With this value, the abundance of C_{60} at 10" from the star is predicted to range between $f_C^{C_{60}} = 3.5 \times 10^{-5}$ and $f_C^{C_{60}} = 2.6 \times 10^{-3}$, in good agreement with the value derived by Berné & Tielens (2012) of $f_C^{C_{60}} = 1.7 \times 10^{-4}$. The comparison can be extended to the other positions (15, 20, and 25") at which the abundance of C_{60} has been measured. At these three positions, the model-derived ranges of abundance also agree well with the observed abundances. However, with increasing distance, the range of acceptable values predicted by the model becomes broader and less constraining. Overall, this comparison demonstrates that our scenario is compatible with observations within the uncertainties on the molecular parameters and the age of the nebula.

6. Discussion

6.1. Comparison to other models

Models of C_{60} formation in a top-down mechanism were presented in Berné & Tielens (2012) and Micelotta et al. (2012). The scenarios in these papers are quite similar, the main difference being that Berné & Tielens (2012) considered PAHs as the starting ingredient, while for Micelotta et al. (2012) the starting ingredient are nanometer-sized "arophatic" clusters. In both studies the evolution of the species is described by a "thermal model" (Arrhenius equation), where the driving parameter is the activation energy. For the loss of C atoms at the edge of graphene sheets, Berné & Tielens (2012) used a value tuned to 4.5 eV to obtain reasonable formation efficiencies. But as noted by Micelotta et al. (2012), this value is somewhat arbitrary, and the obtained C_{60} formation efficiencies remain low. To explain the efficient formation of C_{60} in evolved stars, Micelotta et al. (2012) used the results from the molecular dynamics simulations of Zheng et al. (2007) and extracted a unique activation energy of 0.35 eV for the shrinking reaction by loss of C_2. However, this value is a factor of $\sim$ 20 lower than what is generally accepted for this reaction (see Table 1), leading to over-estimations of the rates by many orders of magnitude, casting serious doubts on the conclusions of Micelotta et al. (2012).

In summary, since these simple models do not consider multiple photon absorptions, the molecules never reach the high internal energies necessary for a high formation rate of C_{60} . Therefore, they strongly underestimate the C_{60} formation yields, unless one assumes activation energies that are too low to be physical. Instead, the approach presented here, which includes a complete description of the photochemical processes, allows, using realistic molecular parameters, predicting formation efficiencies that agree with observations.

6.2. Comparison to experimental results of gas-phase cage formation

After we submitted this paper, Zhen et al. (2014) reported experimental results in which they demonstrated that C_{60} can be formed in the gas phase through laser irradiation of larger PAH molecules. These results support the idea put forward here: that C_{60} can be formed following a top-down scheme. However, Zhen et al. (2014) suggested that in some cases the conversion of graphene into cages could involve a prior step of C_2 loss. This contradicts our photochemical model, in which the dissociation by loss of C_2 is less efficient than the folding by many orders of magnitude, and therefore folding always precedes the loss of C_2. This is mainly because the activation energy for folding (which relies on molecular parameters derived from molecular dynamics simulations performed by Lebedeva et al. 2012) is a factor of $\sim$ 2 lower than the activation energy for C_2 loss. More detailed experimental investigation is necessary, in particular to quantify the activation energies involved in the folding and C_2 loss by flakes, so that they can be included in our model.

6.3. Stability of C_{60}

Table 3 demonstrates that C_{60} can reach particularly high internal energies. In this state, fluorescence from thermally excited electronic states becomes a very efficient cooling channel, postponing the dissociation and conferring an increased stability to C_{60} [4]. Hence, in the frame of the top-down mechanism detailed here and because of its remarkable stability, C_{60} is expected to be the most abundant of all fullerenes in highly UV irradiated environments in space. It is interesting to note that similar kinetic stability arguments have been put forward (Fedorov et al. 2011) to explain the high abundance of C_{60} relative to other fullerenes observed in laboratory experiments (Kroto et al. 1985; Krätschmer et al. 1990). As discussed in Sect. 4.2, C_{60} is expected to survive for 10s of Myr in intense radiation fields. In the diffuse ISM, where the radiation field is several orders of magnitude smaller, C_{60} is therefore expected to resist radiation for even longer timescales. In such conditions, other energetic processes must be invoked to destroy C_{60} , such as shocks or cosmic rays.

6.4. Isomerization of C_{60}

Many C_{60} isomers exist, and hence there is no a priori reason for the icosahedral *Ih*-C_{60} to be the one present in the ISM. *Ih*-C_{60} has the lowest energy of all C_{60} isomers, and the closest isomers lie about 2 eV higher in energy (Raghavachari & Rohlfing 1992). Upon UV absorption, the isomerization reaction from any C_{60} isomer towards *Ih*-C_{60} requires only 5.4 eV of activation energy (Yi & Bernholc 1992) and is therefore expected to be fast in the conditions investigated here. Conversely, the isomerization reaction from *Ih*-C_{60} to another C_{60} isomer requires $\sim 5.4 + 2 = 7.4$ eV and will be much slower than the previous reaction. Therefore the population of C_{60} molecules will relatively quickly be dominated by the icosahedral isomer.

7. Conclusions

We have presented the first detailed photochemical modelling of C_{60} formation from PAHs in space following a top-down scheme. This model was calculated for a single molecule ($C_{66}H_{20}$) as a starting point, and the key processes were explicitly described: UV photon absorption (including multiple photon events), radiative cooling, and dissociation. Because the involved activation energies in this top-down mechanism are high (especially for the shrinking steps), multiple photon absorptions dominate the photochemistry. Using the physical conditions that prevail in the NGC 7023 reflection nebula, we found that C_{60} can be formed from $C_{66}H_{20}$ on a timescale of about 10^5 years with a high efficiency in highly irradiated regions. If it is assumed that only PAHs containing between 60 and 66 C atoms are precursors of C_{60} and that PAHs are distributed in a classical size distribution, the comparison between the modelled and observed abundances of C_{60} shows agrees well within the uncertainties of the model. These uncertainties can be reduced once a better characterization of the reaction rates of the cage shrinking is available. While developed for the physical conditions of NGC 7023 as representative of the interstellar medium, the scenario and model described in this paper can also be applied to the irradiated circumstellar gas of planetary nebulae if the physical conditions in these environments can be characterized in detail.

[4] Note that since multiple photon absorptions are rare, most C_{60} molecules in the ISM are situated at much lower internal energies and the population-averaged emission at a given time remains dominated by infrared transitions. The visible emission of C_{60} in the ISM is therefore probably very weak.

Acknowledgements. This work was supported by the CNRS program "Physique et Chimie du Milieu Interstellaire" (PCMI). JM acknowledges the support of the Academy of Finland grant No. 250741, and the support of the University of Franche-Comté through the BQR funding. We also acknowledge support from the European Research Council under the European Union's Seventh Framework Programme ERC-2013-SyG, Grant Agreement n. 610256 NANOCOSMOS. We acknowledge the referee for constructive comments that improved the quality of this manuscript.

References

Abergel, A., Arab, H., Compiègne, M., et al. 2010, A&A, 518, L96
Alecian, E., Catala, C., Wade, G. A., et al. 2008, MNRAS, 385, 391
Alecian, E., Wade, G. A., Catala, C., et al. 2013, MNRAS, 429, 1001
Andersen, J., Gottrup, C., Hansen, K., Hvelplund, P., & Larsson, M. 2001, The European Physical Journal D - Atomic, Molecular, Optical and Plasma Physics, 17, 189
Berkowitz, J. 1999, The Journal of Chemical Physics, 111, 1446
Berné, O., Joblin, C., Deville, Y., et al. 2012, in SF2A-2012: Proceedings of the Annual meeting of the French Society of Astronomy and Astrophysics, ed. S. Boissier, P. de Laverny, N. Nardetto, R. Samadi, D. Valls-Gabaud, & H. Wozniak, 507–512
Berné, O., Mulas, G., & Joblin, C. 2013, A&A, 550, L4
Berné, O. & Tielens, A. G. G. M. 2012, Proceedings of the National Academy of Science, 109, 401
Cami, J., Bernard-Salas, J., Peeters, E., & Malek, S. E. 2010, Science, 329, 1180
Castellanos, P., Berné, O., Sheffer, Y., Wolfire, M. G., & Tielens, A. G. G. M. 2014, ApJ, 794, 83
Cherchneff, I., Barker, J. R., & Tielens, A. G. G. M. 1992, ApJ, 401, 269
Chupka, W. A. & Klots, C. E. 1997, International Journal of Mass Spectrometry and Ion Processes, 167, 595
Chuvilin, A., Kaiser, U., Bichoutskaia, E., Besley, N. A., & Khlobystov, A. N. 2010, Nature Chemistry, 2, 450
Desert, F.-X., Boulanger, F., & Puget, J. L. 1990, A&A, 237, 215
Diaz-Tendero, S., Alcami, M., & Martin, F. 2003, The Journal of Chemical Physics, 119, 5545
Dunk, P. W., Adjizian, J.-J., Kaiser, N. K., et al. 2013, Proceedings of the National Academy of Sciences, 110, 18081
Fedorov, A. S., Fedorov, D. A., Kuzubov, A. A., et al. 2011, Phys. Rev. Lett., 107, 175506
Frenklach, M. & Feigelson, E. D. 1989, ApJ, 341, 372
García-Hernández, D. A., Kameswara Rao, N., & Lambert, D. L. 2011, ApJ, 729, 126
García-Hernández, D. A., Manchado, A., García-Lario, P., et al. 2010, ApJ, 724, L39
Gluch, K., Matt-Leubner, S., Echt, O., et al. 2004, The Journal of Chemical Physics, 121, 2137
Habing, H. J. 1968, Bull. Astron. Inst. Netherlands, 19, 421
Hansen, K., Hoffmann, K., & Campbell, E. E. B. 2003, The Journal of Chemical Physics, 119
Heath, J. R. 1992, in Fullerenes, ed. G. Hammond & V. Kuck, 1–23
Hunter, J. M., Fye, J. L., Roskamp, E. J., & Jarrold, M. F. 1994, The Journal of Physical Chemistry, 98, 1810
Irle, S., Zheng, G., Wang, Z., & Morokuma, K. 2006, The Journal of Physical Chemistry B, 110, 14531, pMID: 16869552
Joblin, C., Leger, A., & Martin, P. 1992, ApJ, 393, L79
Joblin, C. & Tielens, A. G. G. M., eds. 2011, EAS Publications Series, Vol. 46, PAHs and the Universe: A Symposium to Celebrate the 25th Anniversary of the PAH Hypothesis
Joblin, C., Toublanc, D., Boissel, P., & Tielens, A. G. G. M. 2002, Molecular Physics, 100, 3595
Klots, C. 1991, Zeitschrift fr Physik D Atoms, Molecules and Clusters, 21, 335
Krätschmer, W., Lambl, L. D., Fostiropoulos, K., & Huffmanl, D. R. 1990, Nature, 347
Kroto, H. W., Heath, J. R., Obrien, S. C., Curl, R. F., & Smalley, R. E. 1985, Nature, 318, 162
Kroto, H. W. & McKay, K. 1988, Nature, 331, 328
Laskin, J., Weickhardt, C., & Lifshitz, C. 1997, International Journal of Mass Spectrometry and Ion Processes, 161, L7
Lebedeva, I. V., Knizhnik, A. A., Popov, A. M., & Potapkin, B. V. 2012, The Journal of Physical Chemistry C, 116, 6572
Léger, A., Boissel, P., & d'Hendecourt, L. 1988, Phys. Rev. Lett., 60, 921
Malloci, G., Joblin, C., & Mulas, G. 2007, Chemical Physics, 332, 353
Martin, S., Bernard, J., Brédy, R., et al. 2013, Phys. Rev. Lett., 110, 063003

Matt, S., Echt, O., Scheier, P., & Mrk, T. 2001, Chemical Physics Letters, 348, 194
Matt, S., Parajuli, R., Stamatovic, A., et al. 1999, European Journal of Mass Spectrometry, 5, 477
Merino, P., Švec, M., Martinez, J. I., et al. 2014, Nature Communications, 5
Micelotta, E. R., Jones, A. P., Cami, J., et al. 2012, ApJ, 761, 35
Montillaud, J., Joblin, C., & Toublanc, D. 2013, A&A, 552, A15
Patra, N., Král, P., & Sadeghpour, H. R. 2014, ApJ, 785, 6
Pietrucci, F. & Andreoni, W. 2014, Journal of Chemical Theory and Computation, 10, 913
Pilleri, P., Herberth, D., Giesen, T. F., et al. 2009, MNRAS, 397, 1053
Pilleri, P., Montillaud, J., Berné, O., & Joblin, C. 2012, A&A, 542, A69
Planck Collaboration XXV. 2011, A&A, 536, A25
Raghavachari, K. & Rohlfing, C. M. 1992, The Journal of Physical Chemistry, 96, 2463
Schettino, V., Pagliai, M., Ciabini, L., & Cardini, G. 2001, The Journal of Physical Chemistry A, 105, 11192
Seifert, G., Vietze, K., & Schmidt, R. 1996, Journal of Physics B: Atomic, Molecular and Optical Physics, 29, 5183
Sellgren, K., Werner, M. W., Ingalls, J. G., et al. 2010, Astrophys. J., 722, L54
Slanina, Z. & Lee, S.-L. 1994, Journal of Molecular Structure: {THEOCHEM}, 304, 173
Tielens, A. G. G. M. 2008, ARA&A, 46, 289
Tomita, S., Andersen, J., Hansen, K., & Hvelplund, P. 2003, Chemical Physics Letters, 382, 120
Yi, J.-Y. & Bernholc, J. 1992, The Journal of Chemical Physics, 96
Yi, J.-Y. & Bernholc, J. 1993, Phys. Rev. B, 48, 5724
Zhang, B. L., Xu, C. H., Wang, C. Z., Chan, C. T., & Ho, K. M. 1992, Phys. Rev. B, 46, 7333
Zhang, J., Bowles, F. L., Bearden, D. W., et al. 2013, Nature Chemistry, 5, 880
Zhen, J., Castellanos, P., Paardekooper, D. M., Linnartz, H., & Tielens, A. G. G. M. 2014, ApJ, 797, L30
Zheng, G., Wang, Z., Irle, S., & Morokuma, K. 2007, Journal of Nanoscience and Nanotechnology, 7, 4
Zope, R. R., Baruah, T., Pederson, M. R., & Dunlap, B. I. 2008, Phys. Rev. B, 77, 115452